Supplementary Information

Rational Molecular Design of TADF Emitters towards Highly Efficient Yellow Electroluminescence with nearly 30% External Quantum Efficiency and Low Roll-Off

Honghui Xie, Zhongyan Huang*, Nengquan Li*, Tao Hua, Jingsheng Miao, Chuluo Yang*

Shenzhen Key Laboratory of New Information Display and Storage Materials, College of Materials Science and Engineering, Shenzhen University, Shenzhen 518060, People's Republic of China

Corresponding Authors
Zhongyan Huang, Email: zyhuang@szu.edu.cn
Nengquan Li, Email: lnq0518 @szu.edu.cn
Chuluo Yang, Email: clyang@szu.edu.cn

General characterization. All of the reactions were conducted under the protection of the dry-argon atmosphere. Bruker Advance 400 spectrometer and Bruker Advance 600 spectrometer were used for the ^{1}H and ^{13}C NMR spectrum, respectively. Tetramethylsilane was used as the internal standard and $CDCl_3$ as the solvent. The high resolution mass spectrometry (HR-MS) was determined on a Thermo Scientific LTQ Orbitrap XL with ESI source. The absolute configuration of PXZBO1 and PXZBO2 were confirmed using Bruker D8 Venture diffractometer using MoK radiation (λ = 0.71073) source. The single crystals of the new two emitters were prepared from a saturated dichloromethane and ethanol solution by evaporation method.

Photophysical Characterization: Shimadzu UV-2700 spectrophotometer (Shimadzu, Japan) was applied to record UV-vis spectra at 25 ºC. Photoluminescence (PL) spectra were determined on a Hitachi F-7100 fluorescence spectrophotometer (Hitachi, Japan) at 25 ºC. Phosphorescence spectra (Phos) were recorded on the Hitachi F-7100 fluorescence spectrophotometer at 77 K. The transient PL decay curves were obtained by FluoTime 300 (PicoQuant GmbH) with a Picosecond Pulsed UV-LASTER (LASTER375) as the excitation source. The photoluminescence quantum yields (Φ_{PLQYs}) were achieved by a Hamamatsu UV-NIR absolute PL quantum yield spectrometer (C13534, Hamamatsu Photonics) equipped with a calibrated integrating sphere, the integrating sphere was purged with dry argon to maintain an inert atmosphere.

Thermal Characterization: A TGA Q50 (TA instrument) thermal analysis system

was employed to analyze thermal gravimetric analysis (TGA) ranging from 50 ºC to 800 ºC with a heating rate of 10 K min^{-1} under nitrogen flushing.

Electrochemical Characterization: Cyclic voltammograms (CV) were obtained in dichloromethane at room temperature with a CHI600 electrochemical workstation at 25 ºC and a scan speed of 50 mV s^{-1}. The electrochemical oxidation potentials were collected by cyclic voltammetry measurements via a CHI660 electrochemical workstation (Chenhua, China) and ferroceniumferrocene (Fc/Fc^{+}) was used as the internal reference, tetrabutylammonium hexafluorophosphate (0.1 M) was used as the supporting electrolyte. A platinum plate electrode was utilized as the working electrode, a platinum wire was utilized as the counter electrode and Ag/AgCl as reference electrode. The reduction potentials were calculated from $E_{ox} - E_g$, the optical bandgaps (E_g) were estimated from the onset of the absorption spectra.

Quantum Chemical Calculations: quantum chemical calculations were performed by the Gaussian 09 program package, density functional theory (DFT) using the B3LYP/6-31G(d) was performed for achieved optimized molecular geometries. Based on the optimized geometric configurations, the dihedral angles of these molecules and the highest occupied molecular orbital (HOMO), as well as the lowest unoccupied molecular orbital (LUMO) were obtained logically. Time-dependent DFT (TD-DFT) calculations at the B3LYP/6-31G(d) level were performed to obtain the vertical transitions of the S_1 and T_1 states based on the corresponding S_0 geometries at the same theoretical level.

Analysis of Rate Constants: The rate constants of radiative decay ($k_{r,S}$) and

nonradiative decay ($k_{nr,S}$) from S_1 to S_0 states, the rate constants of intersystem crossing (k_{ISC}) and reverse intersystem crossing (k_{RISC}) were calculated from the following six equations:

$$k_p = 1/\tau_p \quad \text{Eq.(1)}$$

$$k_d = 1/\tau_d \quad \text{Eq.(2)}$$

$$k_{r,S} = \Phi_p k_p + \Phi_d k_d \approx \Phi_p k_p \quad \text{Eq.(3)}$$

$$k_{nr,S} = \frac{1 - \Phi_{PL}}{\Phi_{PL}} k_{r,S} \quad \text{Eq.(4)}$$

$$k_{ISC} = k_p - k_{r,S} - k_{nr,S} \quad \text{Eq.(5)}$$

$$k_{RISC} = (k_p k_d \Phi_d)/(k_{ISC} \Phi_p) \quad \text{Eq.(6)}$$

Where τ_p and τ_d represent the prompt and decay fluorescence lifetime, which determined from transient PL spectra. The k_p and k_d represent the decay rate constants for prompt and delayed fluorescence, respectively. Φ_p and Φ_d indicate prompt and delayed fluorescence components and can be distinguished from the total Φ_{PL} by comparing the integrated intensities of prompt and delayed components in the transient PL spectra.

Device Fabrication and Measurement: To evaluate the EL performance of PXZBO1 and PXZBO2 as emitter materials, we fabricated multilayered TADF OLEDs. All of the small molecular organic materials were purchased (except for the TADF emitters) and purification by temperature-gradient sublimation under vacuum condition. ITO glass substrates were washed sequentially with acetone, deionized

water and isopropyl alcohol in an ultrasonic cleaner, then dried with N_2 flow and finally transferred into a vacuum chamber for deposition. The organic layers of 8-hydroxyquinolinolato-lithium (Liq) and aluminum (Al) were deposited by thermal evaporation at 5×10^{-5} Pa with rates of 0.1 and 3 Å/s, respectively. The other organic layers were deposited at the rates of 0.2-3 Å/s. The emitting area of the device is about 0.09 cm^2. The current density-voltage-luminance (*J-V-L*), *L-EQE* curves and electroluminescence (EL) spectra were measured by using a Keithley 2400 source meter and an absolute EQE measurement system (C9920-12, Hamamatsu Photonics, Japan)

Synthesis and characterization

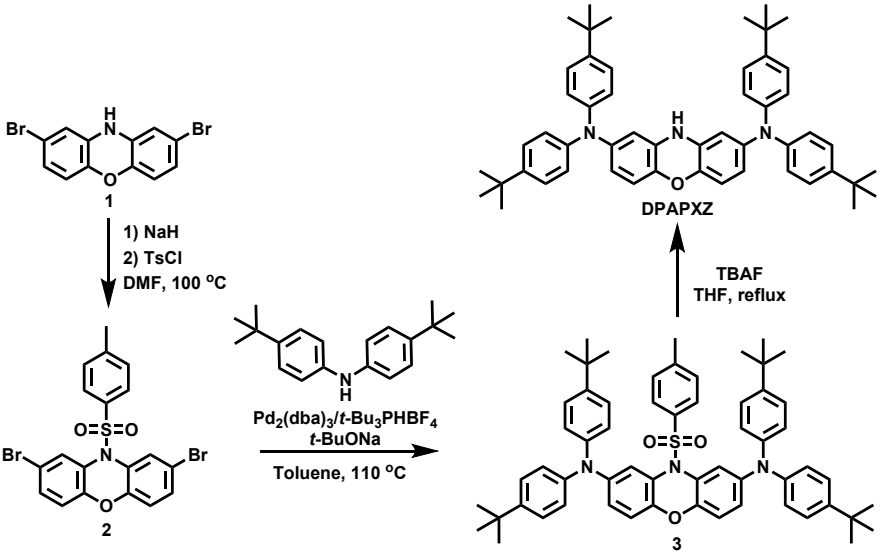

Scheme S1. The synthetic routes of the donor DPAPXZ.

*Synthesis of 2,8-dibromo-10-tosyl-10H-phenoxazine (**2**)*

To a solution of 2,8-dibromo-10*H*-phenoxazine (3.41 g, 10 mmol) in 20 mL DMF was added NaH (0.48 g, 12 mmol) portion-wise at room temperature, after stir at room temperature for another 30 min, tosyl chloride (2.10 g, 11 mmol) was added.

The final mixture was stirred at 100 ºC for 4 h. After cooling to room temperature, the mixture was diluted with ethyl acetate and washed with water for 3 times. Then the diluted solvent was dried over Na_2SO_4 for 15 min and removed by a rotatory evaporation. The crude product was purified by silica gel column chromatography to give compound **2** as a white solid (4.0 g, 81%). ^{1}H NMR (400 MHz, $CDCl_3$) δ (ppm): 7.80 (d, *J* = 2.4 Hz, 2H), 7.32 (dd, *J* = 8.8, *J* = 2.4 Hz, 2H), 7.09-7.03 (m, 4H), 6.68 (d, *J* = 8.8 Hz, 2H), 2.37 (s, 3H).

*Synthesis of N^2,N^2,N^8,N^8-tetrakis(4-(tert-butyl)phenyl)-10-tosyl-10H-phenoxazine-2,8-diamine (**3**)*

Under argon atmosphere, intermediate **2** (2.48 g, 5 mmol), bis(4-(*tert*-butyl)phenyl)amine (3.1 g, 11 mmol), $Pd_2(dba)_3$ (92 mg, 0.1 mmol), *t*-Bu_3PHBF_4 (58 mg, 0.2 mmol), and *t*-BuONa (1.15 g, 12 mmol) were added into a 100 mL two-neck flask charged, 25 mL degassed toluene was injected into the mixture. The reaction was refluxed for 12 h at 110 ºC. After cooled to room temperature, the mixture was diluted with dichloromethane and washed with water for 3 times. Then the diluted solvent was dried over Na_2SO_4 for 15 min and removed by a rotatory evaporation. The crude product was purified by silica gel column chromatography to give the intermediate **3** as a white solid (3.0 g, 67%). ^{1}H NMR (400 MHz, $CDCl_3$) δ (ppm): 7.36 (d, *J* = 2.8 Hz, 2H), 7.28-7.24 (m, 8H), 7.17-7.13 (m, 4H), 7.03-6.99 (m, 8H), 6.89 (dd, *J* = 8.8, *J* = 2.8 Hz, 2H), 6.63 (d, *J* = 8.8 Hz, 2H), 2.40 (s, 3H), 1.31 (s, 36H).

Synthesis of N^2,N^2,N^8,N^8-tetrakis(4-(tert-butyl)phenyl)-10H-phenoxazine- 2,8-diamine (DPAPXZ)

Under argon atmosphere, tetrabutylammonium fluoride (TBAF, 1 mol/L in tetrahydrofuran (THF)) (9.2 mL, 12 mmol) was added into a solution of intermediate **3** (2.69 g, 3 mmol) in 25 mL super-dry THF at room temperature. After the reaction was refluxed for 24 h. The reaction was cooled to room temperature, 100 mL water was added to the mixture. Then the mixture was filtered and the residue was washed with water and ethanol for 3 times. The crude product was purified by silica gel column chromatography to give the target product DPAPXZ as a gray solid (0.89 g, 40%). ^{1}H NMR (400 MHz, $PhCD_3$) δ (ppm): 7.22 (d, *J* = 8.8 Hz, 8H), 7.14 (d, *J* = 8.8 Hz, 8H), 6.52 (d, *J* = 8.8 Hz, 28H), 6.39 (dd, *J* = 8.8, 2.0 Hz, 2H), 5.93 (d, *J* = 2.0 Hz, 2H), 3.58 (brs, 1H), 1.29 (s, 36H). ^{13}C NMR (101 MHz, $PhCD_3$) δ (ppm): 145.79, 144.85, 143.96, 139.32, 131.73, 125.98, 123.77, 116.44, 115.90, 109.70, 33.96, 31.23.

Synthesis of 10-(2,12-di-*tert*-butyl-5,9-dioxa-13*b*-boranaphtho[3,2,1-*de*]anthracen-7-yl)-10*H*-phenoxazine (PXZBO1)

To a solution of phenoazine (1.4 g, 7.5 mmol) and TDBA-Br (2.3 g, 5 mmol) in 30 mL toluene, sodium *tert*-butoxide (0.96 g, 10 mmol) and tri-*tert*-butylphosphine/HBF_4 (0.072 g, 0.25 mmol) were added and the mixture was stirred at 80 °C for 15 min. After that tris(dibenzylideneacetone)dipalladium ($Pd_2(dba)_3$) (0.092 g, 0.1 mmol) was added into the mixture and the reaction was heated to 120 °C for 12 h. The cooling mixture was diluted with ethyl acetate and washed by water and brine. After removing the organic solvent, the residue was purified by silica gel column chromatography with petroleum ether/dichloromethane (v/v = 5/1) to afford a yellow solid (2.4 g,

85%). ^{1}H NMR (400 MHz, $CDCl_3$) δ (ppm): 8.78 (d, *J* = 2.5 Hz, 2H), 7.80 (dd, *J* = 8.8, 2.4 Hz, 2H), 7.50 (d, *J* = 8.8 Hz, 2H), 7.18 (s, 2H), 6.97–6.27 (m, 6H), 6.06 (m, 2H), 1.50 (s, 18H). ^{13}C NMR (125 MHz, $CDCl_3$) δ (ppm): 159.42, 158.68, 145.41, 144.81, 143.99, 133.86, 131.80, 130.27, 123.31, 121.68, 118.03, 115.55, 114.76, 113.76, 110.26, 34.59, 31.54. HRMS $(M + H)^+$ calcd for $C_{38}H_{35}BNO_3$ 564.27100, found: 564.27039.

Synthesis of N^2,N^2,N^8,N^8-tetrakis(4-(*tert*-butyl)phenyl)-10-(2,12-di-*tert*-butyl-5,9-dioxa-13*b*-boranaphtho[3,2,1-*de*]anthracen-7-yl)-10*H*-phenoxazine-2,8-diamine (PXZBO2)

PXZBO2 was synthesized according to procedure similar to PXZBO1 with intermediate of DPAPXZ (1.63g, 2.2 mmol), TDBA-Br (0.92 g, 2 mmol), sodium *tert*-butoxide (0.38 g, 4 mmol), tri-*tert*-butylphosphine/HBF_4 (0.029 g, 0.1 mmol), and tris(dibenzylideneacetone)dipalladium ($Pd_2(dba)_3$) (0.037 g, 0.04 mmol). PXZBO2 was isolated as a yellow solid (1.8 g, 80%). ^{1}H NMR (400 MHz, $CDCl_3$) δ (ppm): 8.67 (d, *J* = 2.4 Hz, 2H), 7.75 (dd, *J* = 8.8, 2.4 Hz, 2H), 7.45 (d, *J* = 8.8 Hz, 2H), 7.19–6.52 (m, 20H), 5.97 (s, 2H), 1.48 (s, 18H), 1.08 (s, 36H). ^{13}C NMR (125 MHz, $CDCl_3$) δ (ppm): 159.04, 158.55, 145.20, 144.92, 131.47, 130.11, 125.61, 121.63, 118.02, 114.92, 34.53, 33.96, 31.53, 31.23, 29.32. HRMS $(M + H)^+$ calcd for $C_{78}H_{85}BN_3O_3$ 1122.66840, found: 1122.66724.

Table S1 Crystal data and structure refinement for **PXZBO1** (CCDC: 2173173)**.**

Empirical formula	$C_{38}H_{34}BNO_3$
Formula weight	563.47
Temperature/K	170.0
Crystal system	monoclinic
Space group	$P2_1/c$
a/Å	13.0026(7)
b/Å	12.3321(8)
c/Å	19.5261(13)
α/°	90
β/°	107.636(2)
γ/°	90
Volume/Å^3	2983.8(3)
Z	4
ρ_{calc}g/cm^3	1.254
μ/mm^{-1}	0.078
F(000)	1192.0
Crystal size/mm^3	0.15 × 0.08 × 0.05
Radiation	MoKα (λ = 0.71073)
2Θ range for data collection/°	3.962 to 52.798
Index ranges	-16 ≤ h ≤ 16, -15 ≤ k ≤ 14, -24 ≤ l ≤ 23
Reflections collected	22161
Independent reflections	6049 [R_{int} = 0.0885, R_{sigma} = 0.0867]
Data/restraints/parameters	6049/0/394
Goodness-of-fit on F^2	1.004
Final R indexes [I>=2σ (I)]	R_1 = 0.0601, wR_2 = 0.1437
Final R indexes [all data]	R1 = 0.1234, wR_2 = 0.1878
Largest diff. peak/hole / e Å-3	0.21/-0.25

Table S2 Crystal data and structure refinement for **PXZBO2** (CCDC: 2173174).

Empirical formula	$C_{78}H_{84}BN_3O_3$
Formula weight	1122.29
Temperature/K	170.0
Crystal system	triclinic
Space group	P-1
a/Å	9.2795(7)
b/Å	16.9611(11)
c/Å	21.8944(15)
α/°	110.360(2)
β/°	93.079(3)
γ/°	91.507(2)
Volume/Å^3	3222.3(4)
Z	2
ρ_{calc}g/cm^3	1.157
μ/mm^{-1}	0.069
F(000)	1204.0
Crystal size/mm^3	0.15 × 0.08 × 0.03
Radiation	MoKα (λ = 0.71073)
2Θ range for data collection/°	3.978 to 52.79
Index ranges	-11 ≤ h ≤ 10, -21 ≤ k ≤ 21, -26 ≤ l ≤ 27
Reflections collected	34698
Independent reflections	12898 [R_{int} = 0.0634, R_{sigma} = 0.0845]
Data/restraints/parameters	12898/18/814
Goodness-of-fit on F^2	1.017
Final R indexes [I>=2σ (I)]	R_1 = 0.0602, wR_2 = 0.1245
Final R indexes [all data]	R_1 = 0.1227, wR_2 = 0.1595
Largest diff. peak/hole / e Å-3	0.41/-0.26

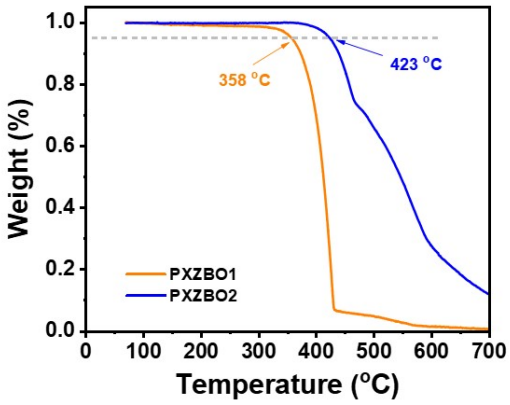

Figure S1. The TGA curves of PXZBO1 and PXZBO2.

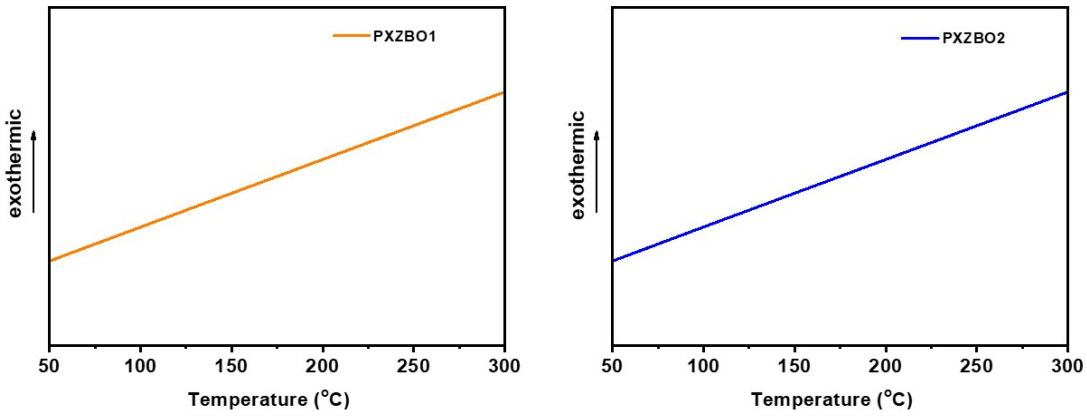

Figure S2. The DSC curves of PXZBO1 and PXZBO2.

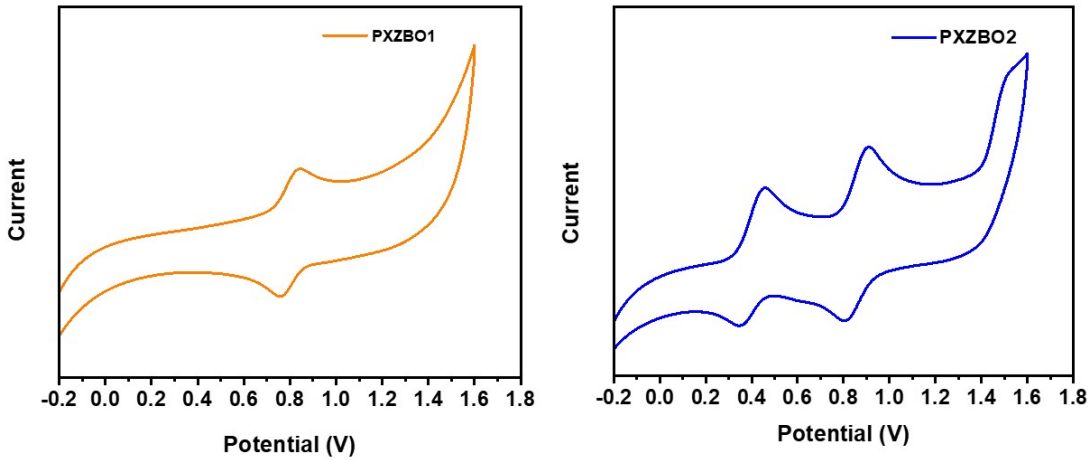

Figure S3. The Cyclic voltammetry curves of PXZBO1 and PXZBO2.

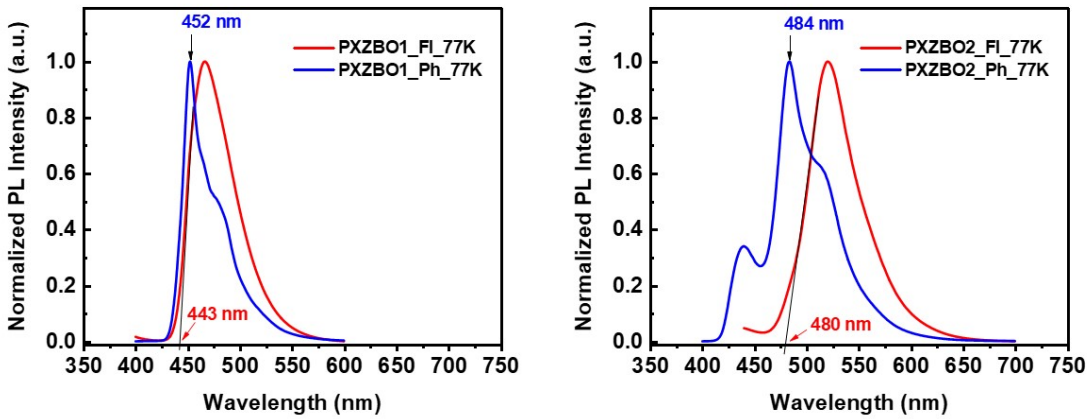

Figure S4. The low temperature (77 K) fluorescent spectra (Fl) and phosphorescent spectra (Phos) of PXZBO1 and PXZBO2 in toluene solution.

Table S3. Summary of photophysical properties and rate constants of PXZBO1 and PXZBO2 in DBFPO films.

Emitter	Delayed ratio	Φ_{DF}	k_p ($\times 10^7$ s^{-1})	k_d ($\times 10^5$ s^{-1})	$k_{r,s}$ ($\times 10^7$ s^{-1})	$k_{nr,s}$ ($\times 10^5$ s^{-1})	k_{ISC} ($\times 10^7$ s^{-1})	k_{RISC} ($\times 10^6$ s^{-1})
PXZBO1	67%	63%	4.26	8.00	1.37	8.75	2.85	2.42
PXZBO2	65%	63%	3.39	5.21	1.18	3.66	2.20	1.49

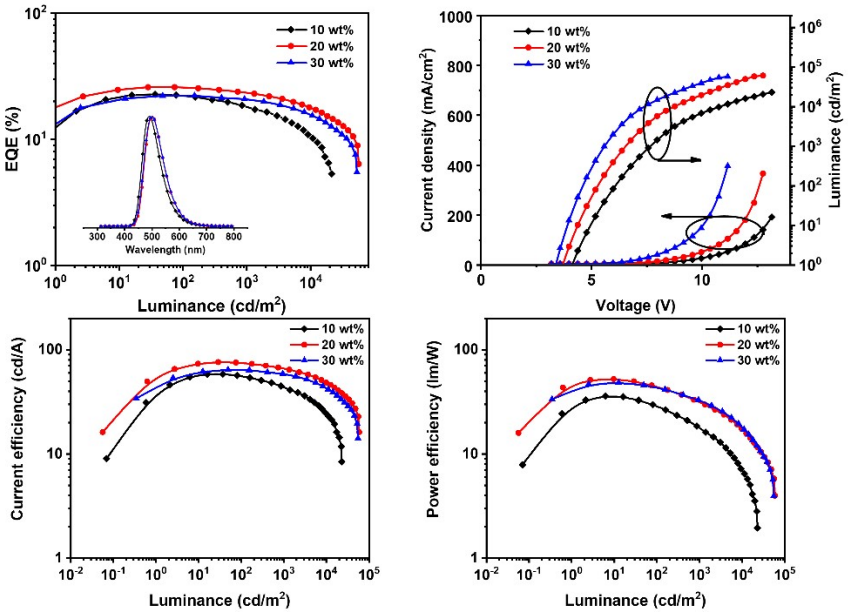

Figure S5. The EL spectra, EQE-luminance curves, current density and luminance versus voltage (*J*-V-L), current efficiency versus luminance and power efficiency versus luminance characteristics of PXZBO1-based devices.

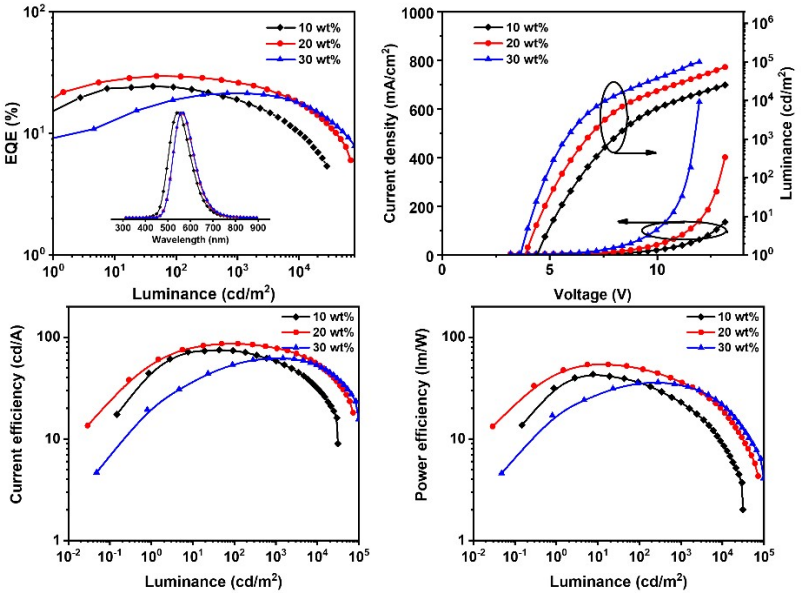

Figure S6. The EL spectra, EQE-luminance curves, current density and luminance versus voltage (*J*-V-L), current efficiency versus luminance and power efficiency versus luminance characteristics of PXZBO2-based devices.

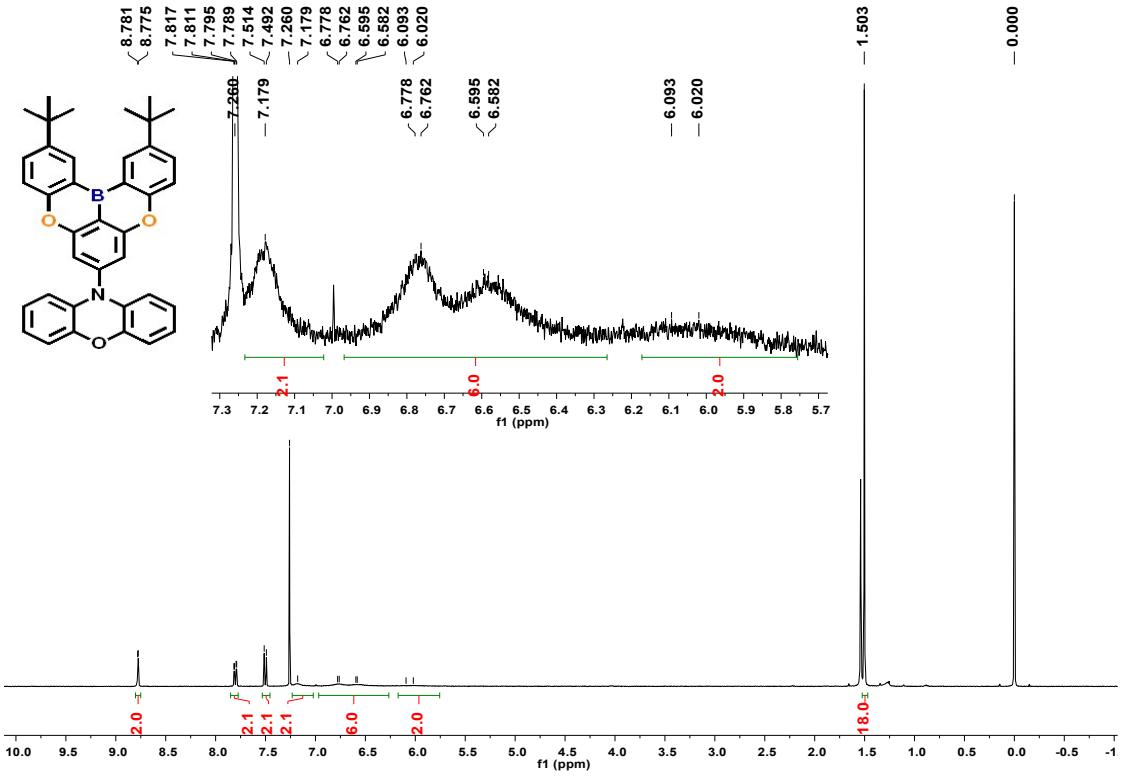

Figure S7. ^{1}H NMR spectrum of PXZBO1.

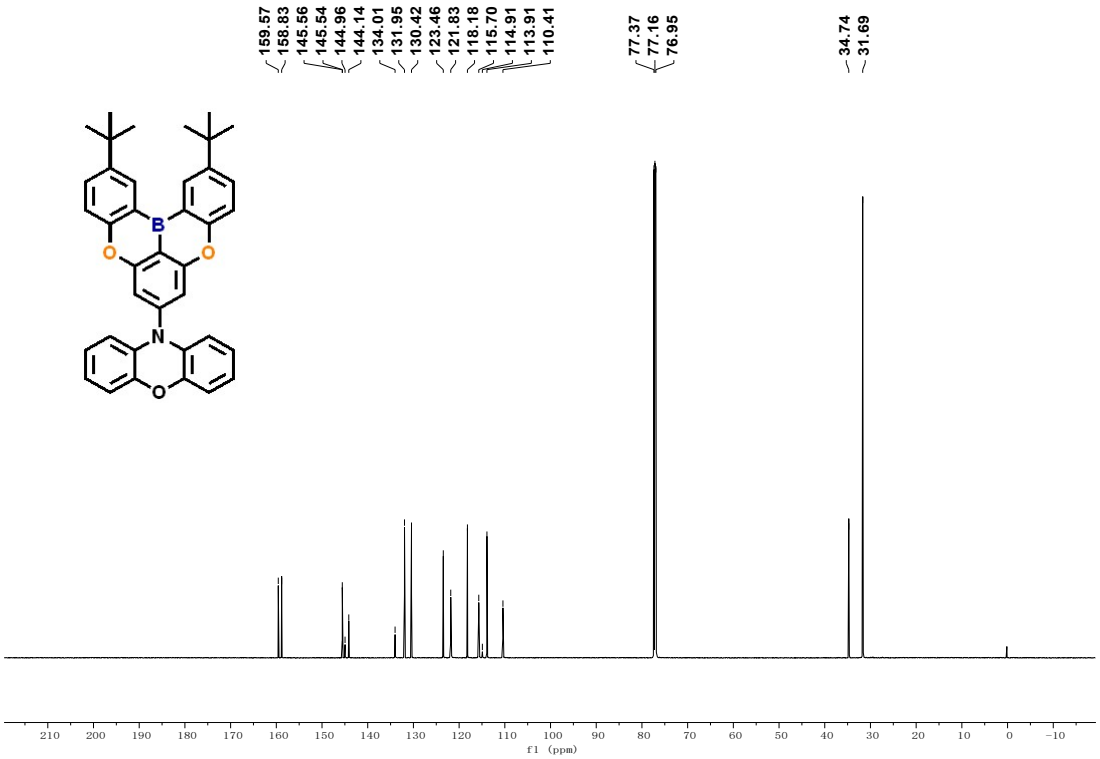

Figure S8. ^{13}C NMR spectrum of PXZBO1.

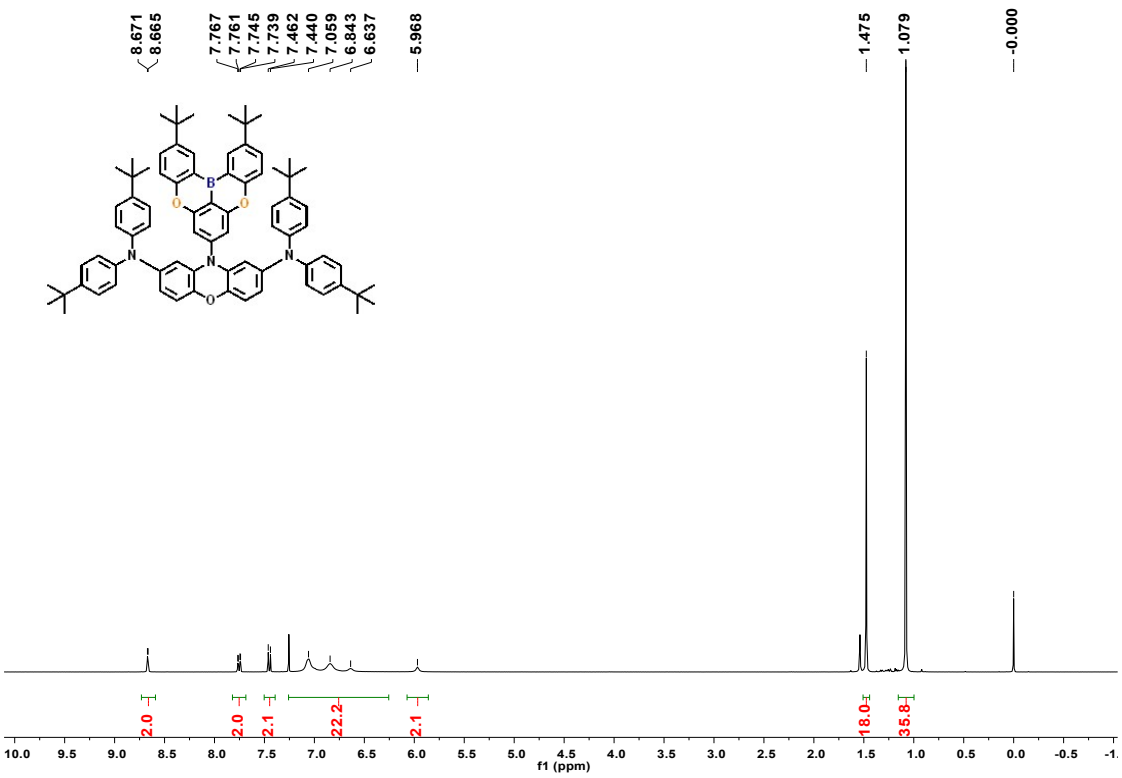

Figure S9. ^{1}H NMR spectrum of PXZBO2.

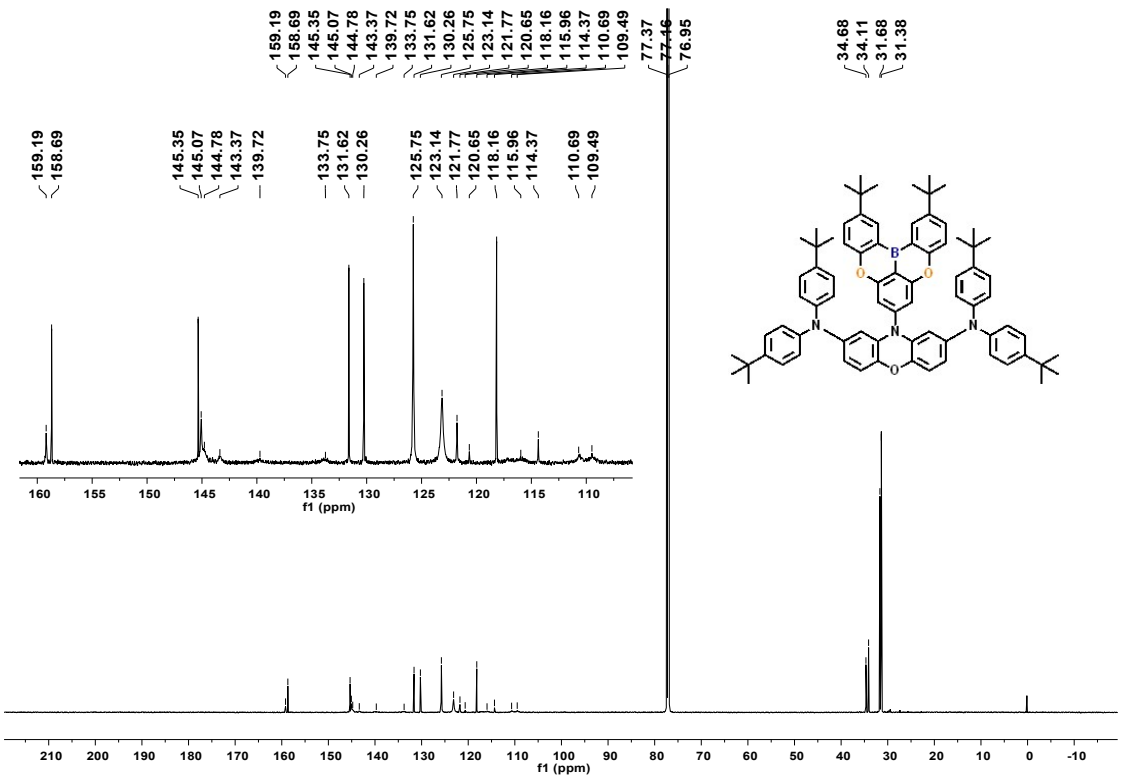

Figure S10. ^{13}C NMR spectrum of PXZBO2.

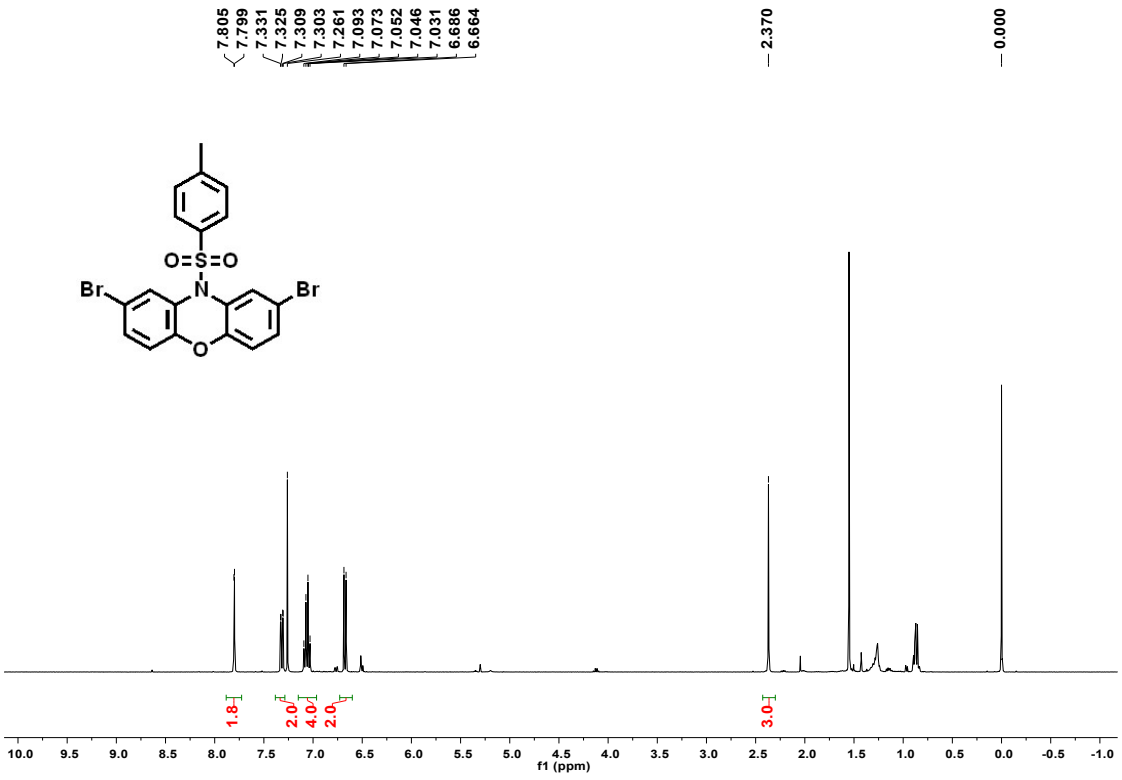

Figure S11. ^{1}H NMR spectrum of intermediate **2**.

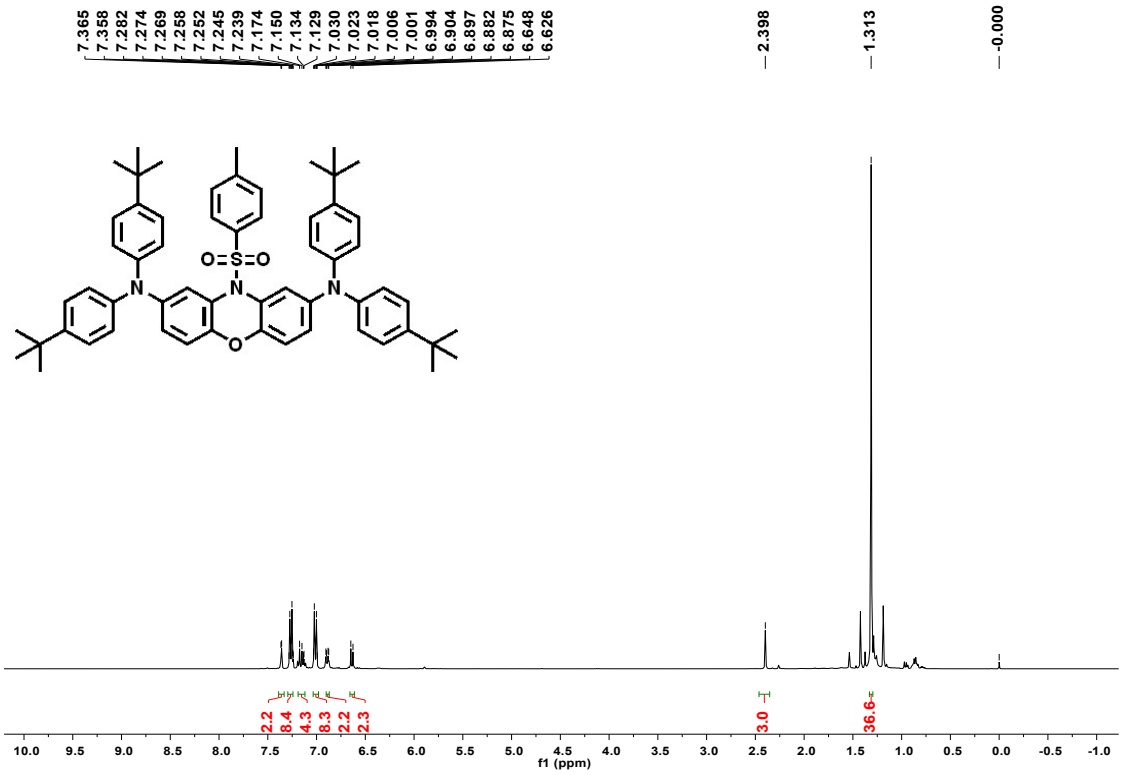

Figure S12. [1]H NMR spectrum of intermediate **3**.

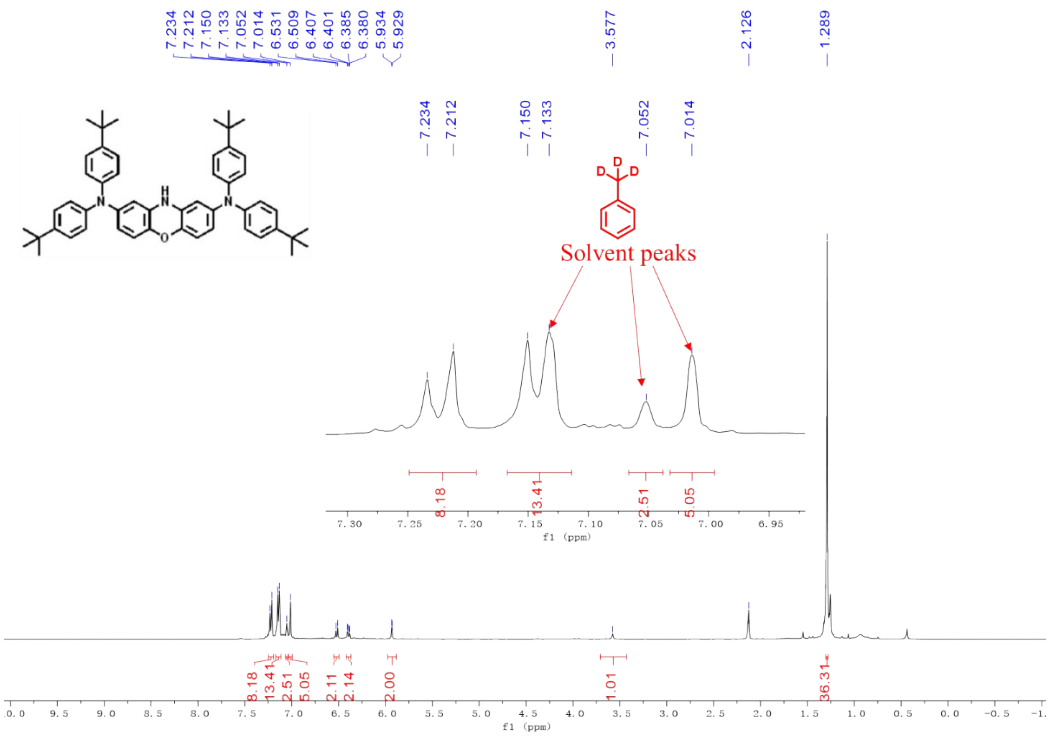

Figure S13. [1]H NMR spectrum of intermediate DPAPXZ.

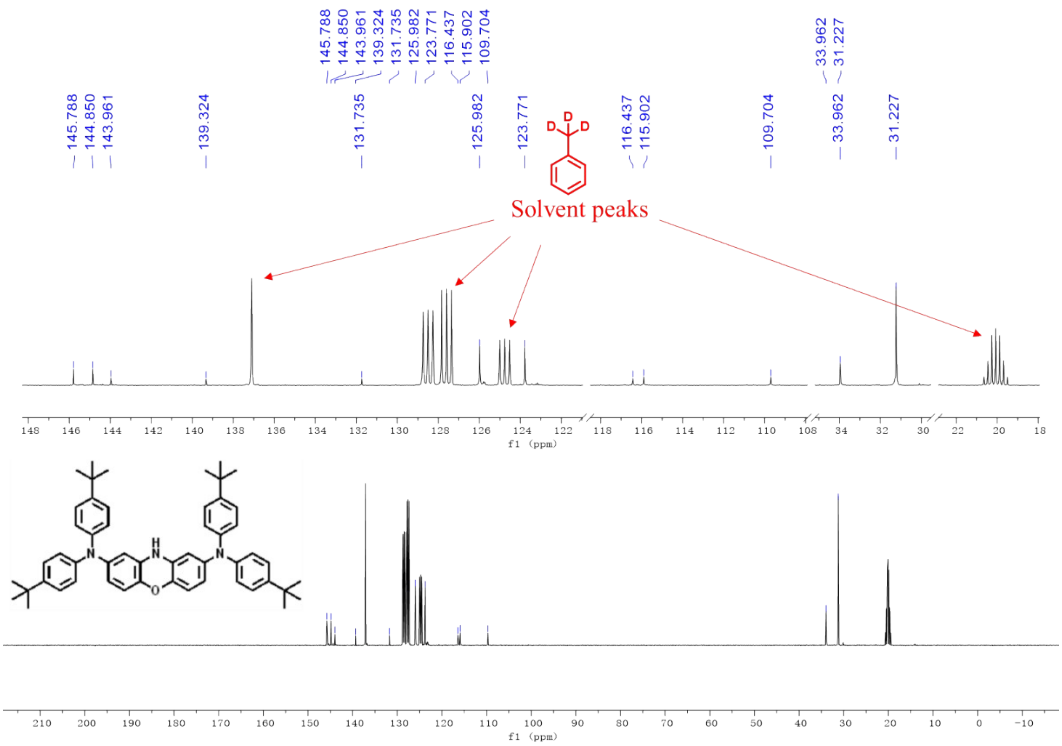

Figure S14. [13]C NMR spectrum of intermediate DPAPXZ.

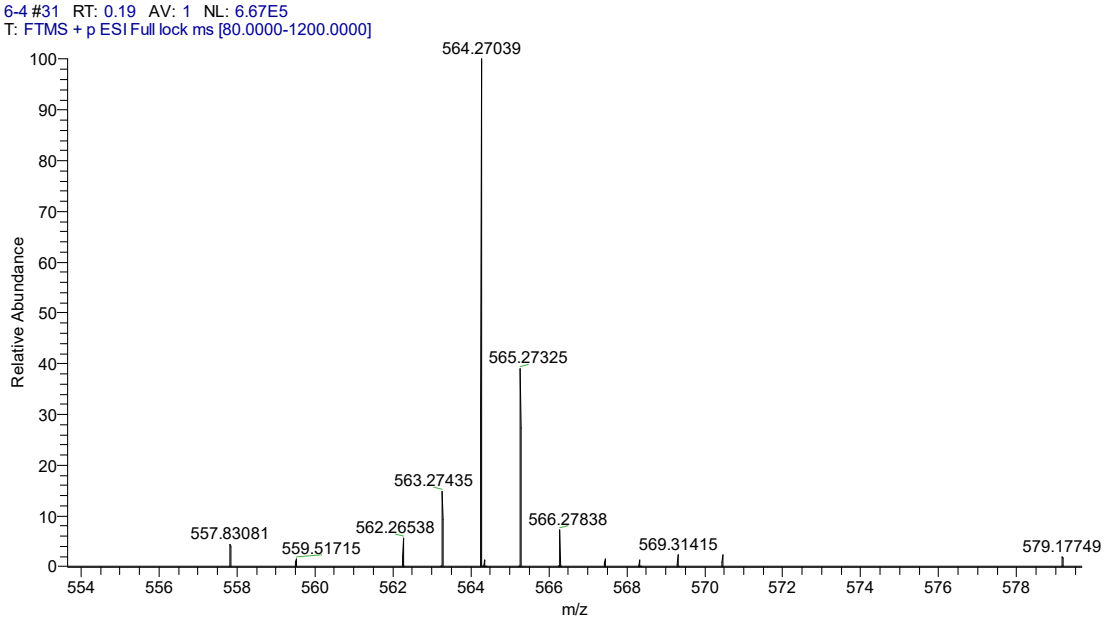

Figure S15. HR-MS spectrum of PXZBO1.

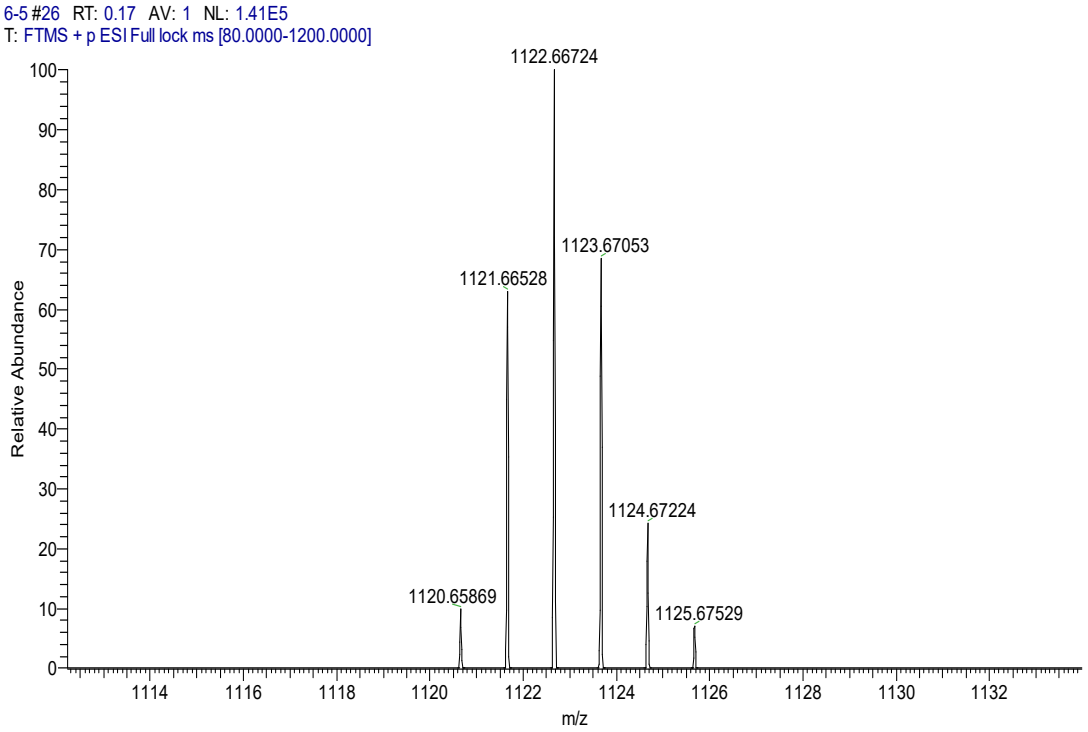

Figure S16. HR-MS spectrum of PXZBO2.